**Smart Structures and Systems**, *Vol. 30, No. 3 (2022) 273-286*
https://doi.org/10.12989/sss.2022.30.3.273


# Identification of structural systems and excitations using vision-based displacement measurements and substructure approach

Ying Lei* and Chengkai Qi

*School of Architecture and Civil Engineering, Xiamen University, Xiamen 361005, China*

(*Received June 26, 2022, Revised July 10, 2022, Accepted July 10, 2022*)

**Abstract.** In recent years, vision-based monitoring has received great attention. However, structural identification using vision-based displacement measurements is far less established. Especially, simultaneous identification of structural systems and unknown excitation using vision-based displacement measurements is still a challenging task since the unknown excitations do not appear directly in the observation equations. Moreover, measurement accuracy deteriorates over a wider field of view by vision-based monitoring, so, only a portion of the structure is measured instead of targeting a whole structure when using monocular vision. In this paper, the identification of structural system and excitations using vision-based displacement measurements is investigated. It is based on substructure identification approach to treat of problem of limited field of view of vision-based monitoring. For the identification of a target substructure, substructure interaction forces are treated as unknown inputs. A smoothing extended Kalman filter with unknown inputs without direct feedthrough is proposed for the simultaneous identification of substructure and unknown inputs using vision-based displacement measurements. The smoothing makes the identification robust to measurement noises. The proposed algorithm is first validated by the identification of a three-span continuous beam bridge under an impact load. Then, it is investigated by the more difficult identification of a frame and unknown wind excitation. Both examples validate the good performances of the proposed method.

**Keywords:** displacement measurement; EKF-UI-WDF; force identification; smoothing; structural identification; substructure identification; system without direct feedthrough; vision sensor

## 1. Introduction

Over the past decades, structural health monitoring (SHM) techniques based on structural vibration response data have been widely investigated to assess the structural conditions (Zhang *et al*. 2015, Liu *et al*. 2016, 2021, Lei *et al*. 2017, Wang *et al*. 2021, Ying *et al*. 2021, Ye *et al*. 2022). In the way of obtaining the vibration response data of the structure, past techniques rely on contact sensors, such as accelerometers, strain gauges, linear variable differential transformer (LVDT), etc. However, contact sensors would take considerable cost, time and efforts in the installation and maintenance, but with limited service lives. In recent years, with the remarkable progress of computer vision techniques, the emerging noncontact vision-based displacement sensor system has offered a promising alternative to the conventional contact sensors (Wang *et al*. 2012, Feng and Feng 2016, Yoon *et al*. 2016). Vision-based structural health monitoring has been gathering increasing attention in the SHM community (Ye *et al*. 2016, Feng and Feng 2017, 2018, Dong *et al*. 2018, Kuddus *et al*. 2019, Spencer *et al*. 2019, Tian *et al*. 2019). However, structural identification includes the identification of structural physical parameters for quantitative structural integrity assessment using vision-based displacement measurements is far less established compared with those using the measurements of on-structure sensors. Especially, it is necessary to investigate the simultaneous identification of structural systems and unknown excitation forces using output only vision-based displacement measurements (Feng and Feng 2017, Spencer *et al*. 2019).

Although vision-based sensor system makes multi-point flexible measurement and low cost come true, compromise between field of view and measurement resolution should be considered when only a single camera is used (Busca *et al*. 2014). In order to guarantee a good measurement resolution, instead of targeting a whole structure, multipoint displacements are only measured for a portion of the structure when using the vision sensor with one single camera (monocular vision). Feng and Feng (2017) studied the identification of structural stiffness and excitation forces using noncontact vision-based displacement measurements of a portion of a simply support beam. It is necessary to assumed that the beam has a constant global stiffness. Otherwise, the measured portion of the structural displacements are not sensitive to the variations of far-away element stiffness. How to identify this target part of structure using only the monocular vision-based displacement measurements is the core issue in this paper. In this respect, substructure approach with the idea of divide and conquer is adopted for this task (Weng *et al*. 2020). For the identification of a target substructure in a whole structural system, the interaction forces from the neighboring substructures at the substructural interfaces are unknown

*Corresponding author, Professor,
E-mail: ylei@xmu.edu.cn


http://www.techno-press.org/?journal=sss&subpage=7
ISSN: 1738-1584 (Print), 1738-1991 (Online)

inputs to the target substructure. Zhang and Moon (2012) proposed a substructure-based method for structural flexibility identification based on substructural interface measurements. Li and Hao (2016) presented a substructural interface force identification method based on the FRFs and the orthogonal polynomial expression of interface forces. Yuen and Huang (2018a, b) investigated substructural identification in time and frequency domain, respectively. Rostami *et al*. (2021) used the extended Kalman filter (EKF) as a joint state-parameter-input identification tool to identify the superstructure, the soil-foundation substructure, and the foundation input. The authors (Lei *et al*. 2022, Yang *et al*. 2022) have also studied substructural identification by treating the interface forces to the target substructure as unknown inputs to be identified. Moreover, the identification of each substructure is in parallel since no information is needed to be transferred between the adjacent substructures (Lei *et al*. 2022). However, all these substructural identification methods are mainly based on the measured responses by conventional contact sensors such as accelerometers and strain gauges.

For the substructural identification using vision-based displacement measurements, the unknown substructural interaction forces to a target substructure do not directly appear in the observation equations of displacement measurements, so the target substructure is a system without direct feedthrough (WDF) of unknown inputs. Gillijns and De Moor (2007) proposed a joint estimation method of structural state and input based on minimum variance unbiased estimation (MVUE). Wan *et al*. (2018) extended to the coupled state/input/parameter identification of linear structural systems, which is an extended version of MVUE. In the field of civil engineering, there is far less research on the identification of structural system without direct feedthrough of unknown inputs than that with direct feedthrough. Pan *et al*. (2009) derived a Kalman filter with unknown input without direct feedthrough method (KF-UI-WDF) with a global optimal solution, and later (Pan *et al*. 2016) extended to a general extended Kalman filter for simultaneous estimation of system and unknown inputs. The authors (Lei *et al*. 2020, Huang *et al*. 2021) also developed the generalized KF-UI (GKF-UI) and generalized EKF-UI (GEKF-UI) by adopting the first-order hold (FOH) approach for the unknown inputs in the discretization of structural state equations. However, the identification results are sensitive to the levels of measurement noises. For vision-based sensing, optical noise is a con effect.

To reduce the sensitivity of identification results to measurement noises, smoothing technique has been proposed (Maes *et al*. 2018, 2019, Feng *et al*. 2020, Lagerblad *et al*. 2021), in which more steps around the current step are used to estimate the unknown input and structural state and parameters at the current step, the increase information of measurements makes the identified result more accurate and stable. Maes *et al*. (2019) combined smoothing and two-step filtering to propose a joint input-state-parameter estimation method, but this method was derived under the framework of linear structural system. Recently, Hassanabadi *et al*. (2022) have proposed a smoothing filter based on the MVUE, but the structural parameters need to be known.

This paper contributes to the simultaneous identification of structural systems and unknown excitation forces using output-only vision-based structural displacement measurements. It is based on the parallel substructural identification approach previously presented by the authors and the proposed smoothing EKF-UI-WDF algorithm for the identification of target substructure and the unknown inputs to solve the problems of limited field of view of vision-based monitoring and the sensitivity of identification results to the measurement noises. The identification of three-span continuous beam bridge subjected to impact load via three substructure identification is studied. Furthermore, it is extended to the difficult task of identification of frame structure and unknown wind excitation using vision-based displacement measurements and substructure approach.

The organization of the rest of paper is as follows. In section 2, the parallel substructural identification previously developed by the authors is introduced and the smoothing EKF-UI-WDF algorithm is proposed. In section 3, two numerical identification validations, the identification of a three-span continuous beam subjected to the impact load and the identification of a multi-story shear frame and the unknown wind load are presented. Finally, some conclusions are presented in section 4.

## 2. The smoothing EKF-UI-WDF for substructure identification using vision-based displacements

### *2.1 The substructural approach using vision-based displacements*

One of the cons of vision is that the accuracy deteriorates for multi-point measurements over a wider field of view. To guarantee good measurement resolution, multipoint displacements are only measured for a portion of a structure instead of targeting the whole structure when using monocular vision, as shown in Fig. 1.

However, the measured portion of the structural displacements are not sensitive to the variations of far-away element stiffness. To solve this problem, the parallel substructure identification approach proposed by the authors (Lei *et al*. 2022) is adopted in this paper.

For the identification of the target substructure, the unknown substructural interaction forces from the

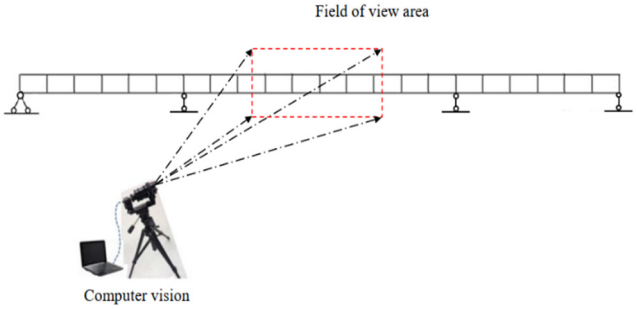


Fig. 1 Schematic of vision-based displacement measurements

neighboring substructures are treated as unknown inputs to the target substructure. Then, the dynamic equation of motion for the target substructure can be formulated as

$$M_s\ddot{x}_s + F_s(x_s, \dot{x}_s, \theta_s) = \eta_{se} f_{se} + \eta_s^u f_s^u \tag{1}$$

in which, the subscript *s* denotes 'substructure', $M_s$ is the substructural mass matrix; $\ddot{x}_s, \dot{x}_s, x_s$ represent the substructural acceleration, velocity and displacement respectively; $\theta_s$ is the unknown substructural parametric vector, $F_s$ is the restoring force vector, which is the function of displacement, velocity and parameters. The right terms in Eq. (1) are

$$\eta_s^u = [\eta_{se}^u \quad \eta_{sb}^u]; \qquad f_s^u = [f_{se}^u \quad f_{sb}^u]^T \tag{2}$$

where subscript "se" and "sb" denote "external" and "boundary" relative to the substructure; $f_{se}$ represents the known external force vector and $\eta_{se}$ is the corresponding force influence matrix, $f_s^u$ represents the unknown force vector containing both the unknown external force $f_{se}^u$ and the unknown interface forces $f_{sb}^u$ to the substructure, and $\eta_s^u$ is influence matrix of unknown force $f_s^u$.

By defining the augmented state vector $Z_s = [x_s^T, \dot{x}_s^T, \theta_s^T]^T$, Eq. (1) can be can rewritten in the state-space as

$$\begin{aligned} \dot{Z}_s &= \begin{bmatrix} \dot{x}_s \\ M_s^{-1}(-F_s(x_s, \dot{x}_s, \theta_s) + \eta_{se} f_{se} + \eta_s^u f_s^u) \\ 0 \end{bmatrix} \\ &= \mathrm{g}(Z_s, f_s) + B^u f_s^u \end{aligned} \tag{3}$$

in which

$$\begin{aligned} g(Z_s, f_s) &= \begin{bmatrix} \dot{x}_s \\ M_s^{-1}(-F_s(x_s, \dot{x}_s, \theta_s) + \eta_{se} f_{se}) \\ 0 \end{bmatrix}; \\ B^u &= \begin{bmatrix} \mathbf{0} \\ M_s^{-1}\eta_s^u \\ \mathbf{0} \end{bmatrix} \end{aligned} \tag{4}$$

For vision-based monitoring on the target substructure, structural dynamic displacement responses are measured. Then, the observing equations can be as

$$y_{s,k+1} = \boldsymbol{S}_d x_s = [\boldsymbol{S}_d \quad 0 \quad 0] \begin{bmatrix} x_s \\ \dot{x}_s \\ \boldsymbol{\theta}_s \end{bmatrix} = \boldsymbol{H} Z_{s,k+1} + v_{k+1} \tag{5}$$

where $\boldsymbol{S}_d$ is the location matrix corresponding to observed DOFs by the computer vision; $\boldsymbol{H} = [\boldsymbol{S}_d \quad 0 \quad 0]$ is a constant matrix; Therefore, the unknown force vector $f_s^u$ does not directly shows in the Eq. (5), i.e., Eq. (5) is a linear function but without direct feedthrough of the unknown force $f_s^u$.

Some researchers including the authors (Pan *et al*. 2016, Lei *et al*. 2020, Huang *et al*. 2021) have developed algorithms for the identification of structural system without direct feedthrough of unknown inputs, However, the identification results are sensitive to the levels of measurement noises.

### *2.2 The proposed smoothing EKF-UI-WDF algorithm*

To reduce the sensitivity of identification results to measurement noises, the smoothing technique is adopted herein.

Let $\hat{Z}_{s,k|k+N-1}$ denotes the estimated value of the $Z_{s,k}$ and the subscript "$k|k+N-1$" denotes the estimation at *k*-th step by using the measurement sequence $[y_1^T \; y_2^T \; \cdots \; y_k^T \; \cdots \; y_{k+N-1}^T]^T$, the nonlinear function Eq. (3) due to the coupling between the unknown parameters and structural state can be linearized by Taylor-expansion at $\hat{Z}_{s,k|k+N-1}$ as

$$\begin{aligned} \dot{Z}_s &= g(Z_s, f_{se}) + B^u f_s^u \\ &\approx \mathrm{g}\big(\hat{Z}_{s,k|k+N-1}, f_{se}\big) + U_k\big(Z_s - \hat{Z}_{s,k|k+N-1}\big) + B^u f_s^u \\ &= U_k Z_s + B^u f_s^u + u_{k,k} \end{aligned} \tag{6}$$

in which

$$\begin{aligned} U_k &= \left.\frac{\partial g(Z_s, f_{se})}{\partial Z_s^T}\right|_{Z_s = \hat{Z}_{s,k|k+N-1}}; \\ u_{k,k} &= g\big(\hat{Z}_{s,k|k+N-1}, f_{se,k}\big) - U_k \hat{Z}_{s,k|k+N-1} \end{aligned} \tag{7}$$

Discretizing the continuous Eq. (6), in which the model error is considered, leads to

$$Z_{s,k+1} = A_k Z_{s,k} + B_k f_{s,k}^u + g_{k,k} + w_k \tag{8}$$

where

$$\begin{aligned} A_k &= e^{U_k \Delta t}; B_k = (A_k - I)(U_k)^{-1} B^u \\ g_{k,k} &= (A_k - I)(U_k)^{-1} u_{k,k} \end{aligned} \tag{9}$$

$\Delta t$ is the sampling interval time; $w_k$ is the model error term with zero mean value and $\boldsymbol{Q}_k$ variance value.

Analogously, the observation equation of Eq. (5) can be expended with the more steps of observed data around the current step. By sequentially substitute Eq. (8) into Eq. (5) in the interval $[(k+1)\Delta t, (k+N)\Delta t]$, the augmented observation equation is derived as

$$\begin{aligned} Y_{s,k+1} = \bar{H}_{k+1} Z_{s,k+1} + \bar{D}_{k+1} F_{s,k+1}^u \\ + \bar{L}_{k+1} \bar{g}_{k+1} + \bar{L}_{k+1} W_{k+1} + V_{k+1} \end{aligned} \tag{10}$$

in which

$$\begin{aligned} Y_{s,k+1} &= \begin{bmatrix} y_{s,k+1} \\ y_{s,k+2} \\ \vdots \\ y_{s,k+N} \end{bmatrix}; \qquad \bar{H}_{k+1} = \begin{bmatrix} H \\ HA_k \\ \vdots \\ HA_k^{N-1} \end{bmatrix}; \\ F_{s,k+1}^u &= \begin{bmatrix} f_{s,k}^u \\ f_{s,k+1}^u \\ \vdots \\ f_{s,k+N-1}^u \end{bmatrix} \\ \bar{D}_{k+1} &= \begin{bmatrix} 0 & 0 & \cdots & 0 \\ 0 & HB_k & \cdots & 0 \\ \vdots & \vdots & \ddots & \vdots \\ 0 & HA_k^{N-1}B_k & \cdots & HB_k \end{bmatrix}; \end{aligned} \tag{11}$$

$$\bar{g}_{k+1}=\begin{bmatrix} g_{k,k} \\ g_{k,k+1} \\ \vdots \\ g_{k,k+N-1} \end{bmatrix}$$

$$\bar{L}_{k+1}=\begin{bmatrix} 0 & 0 & \cdots & 0 \\ 0 & H & \cdots & 0 \\ \vdots & \vdots & \ddots & \vdots \\ 0 & HA_k^{N-1} & \cdots & H \end{bmatrix}; \tag{11}$$

$$W_{k+1}=\begin{bmatrix} w_k \\ w_{k+1} \\ \vdots \\ w_{k+N-1} \end{bmatrix}; \qquad V_{k+1}=\begin{bmatrix} v_{k+1} \\ v_{k+2} \\ \vdots \\ v_{k+N} \end{bmatrix}$$

$$\begin{cases} g_{k,i}=(A_k-I)(U_k)^{-1}u_{k,i} \\ u_{k,i}=g\left(\hat{Z}_{s,k|k+N-1},f_{se,i}\right)-U_k\hat{Z}_{s,k|k+N-1} \\ \qquad\qquad (k\le i\le k+N-1) \end{cases} \tag{12}$$

Therefore, the original observation equation is augmented with the added measurements from step *k*+1 to *k*+*N*. By this way, a more observation information is used for the simultaneous identification of substructural system and the unknown inputs.

The derivation of the proposed smoothing EKF-UI-WDF algorithm is based on the frame of the minimum variance unbiased estimation (MVUE) (Gillijns and De Moor 2007).

By defining $\breve{Z}_{s,k+1|k+N-1}$ from Eq. (8) as

$$\breve{Z}_{s,k+1|k+N-1}\triangleq A_k\hat{Z}_{s,k|k+N-1}+g_{k,k} \tag{13}$$

and $\hat{F}^u_{s,k+1|k+N}$ from Eq. (10) as

$$\hat{F}^u_{s,k+1|k+N}=M_{k+1}\left(Y_{s,k+1}-\bar{H}_{k+1}\breve{Z}_{s,k+1|k+N-1}-\bar{L}_{k+1}\bar{g}_{k+1}\right) \tag{14}$$

in which $M_{k+1}$ is input gain matrix to be determined later, unknown input $\hat{f}^u_{s,k|k+N}$ can be extracted from $\hat{F}^u_{s,k+1|k+N}$ based on the Eq. (11) as

$$\hat{f}^u_{s,k|k+N}=I_F\hat{F}^u_{s,k+1|k+N} \tag{15}$$

where $I_F\triangleq[I \quad 0]$.

From Eq. (8), the predicted state is

$$\tilde{Z}_{s,k+1|k+N-1}=A_k\hat{Z}_{s,k|k+N-1}+B_k\hat{f}^u_{s,k|k+N}+g_{k,k} \tag{16}$$

Then, the updated state can be obtained according to the Eq. (10)

$$\begin{aligned}\hat{Z}_{s,k+1|k+N}=&\tilde{Z}_{s,k+1|k+N-1}\\&+K_{k+1}\left(Y_{s,k+1}-\bar{H}_{k+1}\tilde{Z}_{s,k+1|k+N-1}\right.\\&\left.-\bar{D}_{k+1}\hat{F}^u_{s,k+1|k+N}-\bar{L}_{k+1}\bar{g}_{k+1}\right)\end{aligned} \tag{17}$$

where $K_{k+1}$ is the state gain matrix to be determined later.

Eqs. (13)-(17) are the basic equations of the proposed filter method. However, since the smoothing technique is introduced, the error covariance matrix will be different and more complex.

Section 2.2.1 and 2.2.2 focus on the estimation of input and state, respectively, and section 2.3 presents the recursive estimation of the error covariances (Hassanabadi *et al*. 2022).

### *2.2.1 Estimation of unknown input*

This section first derives the estimation of input gain matrix $M_{k+1}$. Then, the unknown inputs can be estimated through Eqs. (14)-(15) once $M_{k+1}$ is estimated.

#### *1) Unbiased condition*

From Eq. (14), one can define

$$e^Y_{k+1}\triangleq Y_{s,k+1}-\bar{H}_{k+1}\breve{Z}_{s,k+1|k+N-1}-\bar{L}_{k+1}\bar{g}_{k+1} \tag{18}$$

and the error of estimated state is

$$\hat{e}^Z_k\triangleq Z_{s,k}-\hat{Z}_{s,k|k+N-1} \tag{19}$$

By substituting the Eqs. (8), (10) and (13) into the Eq. (18), Eq. (18) can be derived as

$$\begin{aligned} e^Y_{k+1}&=Y_{s,k+1}-\bar{H}_{k+1}\breve{Z}_{s,k+1|k+N-1}-\bar{L}_{k+1}\bar{g}_{k+1}\\&=\bar{H}_{k+1}Z_{s,k+1}+\bar{D}_{k+1}F^u_{s,k+1}+\bar{L}_{k+1}W_{k+1}+V_{k+1}\\&\quad-\bar{H}_{k+1}\left(A_k\hat{Z}_{s,k|k+N-1}+g_{k,k}\right)\\&=\bar{H}_{k+1}\left(A_kZ_{s,k}+B_kf^u_{s,k}+g_{k,k}+w_k\right)\\&\quad+\bar{D}_{k+1}F^u_{s,k+1}+\bar{L}_{k+1}W_{k+1}+V_{k+1}\\&\quad-\bar{\mathrm{H}}_{k+1}\left(A_k\hat{Z}_{s,k|k+N-1}+g_{k,k}\right)\\&=\bar{D}_{k+1}F^u_{s,k+1}+\bar{H}_{k+1}B_kf^u_{s,k}+\bar{H}_{k+1}A_k\hat{e}^Z_k\\&\quad+\bar{H}_{k+1}w_k+\bar{L}_{k+1}W_{k+1}+V_{k+1}\end{aligned} \tag{20}$$

By defining the following terms

$$I_W\triangleq[I \quad 0], \qquad w_k=I_WW_{k+1} \tag{21}$$

$$\begin{aligned}&\Gamma_{k+1}\triangleq\bar{H}_{k+1}A_k;\ \breve{L}_{k+1}\triangleq\bar{L}_{k+1}+\bar{H}_{k+1}I_W\\&\breve{D}_{k+1}\triangleq\bar{D}_{k+1}+\bar{H}_{k+1}B_kI_F\end{aligned} \tag{22}$$

$$e_{k+1}\triangleq\Gamma_{k+1}\hat{e}^Z_k+\breve{L}_{k+1}W_{k+1}+V_{k+1} \tag{23}$$

Eq. (20) can be simplified as

$$e^Y_{k+1}=\breve{D}_{k+1}F^u_{s,k+1}+e_{k+1} \tag{24}$$

According to the principle of the unbiasedness $E\left[\hat{F}^u_{s,k+1|k+N}\right]=F^u_{s,k+1}$, one has the following derivations based on the Eqs. (14) and (24)

$$\begin{aligned}E\left[\hat{F}^u_{s,k+1|k+N}\right]&=M_{k+1}E\left[e^Y_{k+1}\right]\\&=M_{k+1}E\left[\breve{D}_{k+1}F^u_{s,k+1}+e_{k+1}\right]=F^u_{s,k+1}\end{aligned} \tag{25}$$

If the estimated state $\hat{Z}_{s,k|k+N-1}$ is unbiased, which means $E[\hat{e}^Z_k]=0$ and based on the Eq. (23), one has

$$E[e_{k+1}]=E\left[\Gamma_{k+1}\hat{e}^Z_k+\breve{L}_{k+1}W_{k+1}+V_{k+1}\right]=0 \tag{26}$$

By substituting the Eq. (26) into Eq. (25), Eq. (25) can be derived as

$$M_{k+1}E\left[\breve{D}_{k+1}F_{s,k+1}^{u}+e_{k+1}\right] = M_{k+1}\breve{D}_{k+1}F_{s,k+1}^{u} = F_{s,k+1}^{u} \tag{27}$$

Then

$$M_{k+1}\breve{D}_{k+1} = I \tag{28}$$

Eq. (28) is the unbiased condition that make the Eq. (14) unbiased. Actually, one can get the unbiased solution of the unknown input $F_{s,k+1}^{u}$ by using the least-square estimation (LSE) to solve the Eq. (24). However, the solution does not have the minimum-variance since the error term $e_{k+1}$ does not have unit variance according to the Gauss–Markov theorem (Gillijns and De Moor,2007). The minimum-variance unbiased estimation of the unknown input $F_{s,k+1}^{u}$ is shown in the next section.

*2) Minimum-variance condition*

By defining $\tilde{R}_{k+1} \triangleq E[(e_{k+1})(e_{k+1})^T]$, $\tilde{R}_{k+1}$is derived based on Eq. (23) as

$$\tilde{R}_{k+1} = \Gamma_{k+1}\hat{P}_k^Z\Gamma_{k+1}^T + \breve{L}_{k+1}\bar{Q}_k\breve{L}_{k+1}^T + \bar{R}_{k+1} + S\left(\Gamma_{k+1}\hat{P}_k^{ZW}\breve{L}_{k+1}^T\right) + S\left(\Gamma_{k+1}\hat{P}_k^{ZV}\right) \tag{29}$$

where $S(\ \ )$ is a function which satisfies: $S(\boldsymbol{X}) \triangleq \boldsymbol{X}+\boldsymbol{X}^T$ and $\bar{Q}_k = E[(W_{k+1})(W_{k+1})^T]$, $\bar{R}_{k+1} = E[(V_{k+1})(V_{k+1})^T]$, $\hat{P}_k^Z = E[(\hat{e}_k^Z)(\hat{e}_k^Z)^T]$, $\hat{P}_k^{ZW} = E[(\hat{e}_k^Z)(W_{k+1})^T]$ and $\hat{P}_k^{ZV} = E[(\hat{e}_k^Z)(V_{k+1})^T]$.

One can always find an invertible matrix $\tilde{S}_{k+1}$ which satisfies $\tilde{S}_{k+1}\tilde{S}_{k+1}^T = \tilde{R}_{k+1}$. Then, Eq. (24) can be rewritten by multiplying the $\tilde{S}_{k+1}^{-1}$ as

$$\tilde{S}_{k+1}^{-1}e_{k+1}^Y = \tilde{S}_{k+1}^{-1}\breve{D}_{k+1}F_{s,k+1}^{u} + \tilde{S}_{k+1}^{-1}e_{k+1} \tag{3}$$

Obviously, the error term $\tilde{S}_{k+1}^{-1}e_{k+1}$ in Eq. (30) has

$$E\left[\left(\tilde{S}_{k+1}^{-1}e_{k+1}\right)\right] = \mathbf{0};\quad E\left[\left(\tilde{S}_{k+1}^{-1}e_{k+1}\right)\left(\tilde{S}_{k+1}^{-1}e_{k+1}\right)^T\right] = I \tag{31}$$

which means that the Eq. (30) satisfies the Gauss–Markov theorem.

The input gain matrix $M_{k+1}$ corresponding to the Eq. (30) satisfies the unbiased condition by Eq. (28) since the LSE solution of Eq. (30) satisfies $E\left[\hat{F}_{s,k+1|k+N}^{u}\right] = F_{s,k+1}^{u}$. In addition, the error of estimation $\hat{F}_{s,k+1|k+N}^{u}$ from Eq. (30) has the minimum-variance since the error term $\tilde{S}_{k+1}^{-1}e_{k+1}$ has the unit variance according to the Gauss–Markov theorem (Gillijns and De Moor 2007).

The LS solution of Eq. (30) is

$$\hat{F}_{s,k+1|k+N}^{u} = \left(\breve{D}_{k+1}^T\tilde{R}_{k+1}^{-1}\breve{D}_{k+1}\right)^{-1}\breve{D}_{k+1}^T\tilde{R}_{k+1}^{-1}\left(Y_{k+1} - \bar{H}_{k+1}\breve{Z}_{s,k+1|k+N-1} - \bar{L}_{k+1}\bar{g}_{k+1}\right) \tag{32}$$

By comparing Eq. (14), $M_{k+1}$is derived as

$$M_{k+1} = \left(\breve{D}_{k+1}^T\tilde{R}_{k+1}^{-1}\breve{D}_{k+1}\right)^{-1}\breve{D}_{k+1}^T\tilde{R}_{k+1}^{-1} \tag{33}$$

Eq. (33) is the minimum-variance condition of the $M_{k+1}$ needs to satisfy. Meanwhile, Eq. (33) automatically satisfies the unbiased condition by Eq. (28). Therefore, Eq. (32) is the MVUE of the unknown input $F_{s,k+1}^{u}$.

### *2.2.2 Estimation of state*

Similar to the input estimation in the above section, this section aims to estimate the gain matrix $K_{k+1}$, and then the state can be obtained.

*1) Unbiased condition*

By defining the error of the predicted state $\tilde{e}_{k+1}^Z \triangleq Z_{s,k+1} - \tilde{Z}_{s,k+1|k+N-1}$ and the error of estimated input $\hat{e}_{k+1}^F \triangleq F_{s,k+1}^{u} - \hat{F}_{s,k+1|k+N}^{u}$, $\hat{e}_k^f \triangleq f_{s,k}^{u} - \hat{f}_{s,k|k+N}^{u}$, one can derive the recursive form of $\tilde{e}_{k+1}^Z$ from Eq. (8) and Eq. (16) as

$$\tilde{e}_{k+1}^Z = A_k\hat{e}_k^Z + B_k\hat{e}_k^f + w_k \tag{34}$$

From Eq. (14), Eq. (24) and Eq. (28), one can get the following derivation

$$\begin{aligned}\hat{e}_{k+1}^F &= F_{s,k+1}^{u} - \hat{F}_{s,k+1|k+N}^{u}\\ &= F_{s,k+1}^{u} - \left(M_{k+1}\breve{D}_{k+1}F_{s,k+1}^{u} + M_{k+1}e_{k+1}\right)\\ &= -\mathrm{M}_{k+1}e_{k+1}\end{aligned} \tag{35}$$

Based on Eq. (15), Eq. (23) and Eq. (35), $\hat{e}_k^f$ is derived as

$$\begin{aligned}\hat{e}_k^f &= f_{s,k}^{u} - \hat{f}_{s,k|k+N}^{u} = I_F\left(F_{s,k+1}^{u} - \hat{F}_{s,k+1|k+N}^{u}\right)\\ &= I_F\hat{e}_{k+1}^F = -I_FM_{k+1}e_{k+1}\\ &= -I_FM_{k+1}\left(\Gamma_{k+1}\hat{e}_k^Z + \bar{L}_{k+1}W_{k+1} + V_{k+1}\right)\end{aligned} \tag{36}$$

Then, substituting Eq. (36) into Eq. (34) leads to

$$\tilde{e}_{k+1}^Z = A_k^*\hat{e}_k^Z + w_k^* \tag{37}$$

in which $A_k^* \triangleq A_k - G_{k+1}\Gamma_{k+1}$; $w_k^* \triangleq J_{k+1}W_{k+1} - G_{k+1}V_{k+1}$; $G_{k+1} \triangleq B_kI_FM_{k+1}$; $J_{k+1} \triangleq -G_{k+1}\bar{L}_{k+1} + I_W$.

The error of estimated state $\hat{e}_{k+1}^Z$, can be derived from Eq. (8), Eq. (17) and Eq. (24) as

$$\hat{e}_{k+1}^Z = \tilde{e}_{k+1}^Z - K_{k+1}\left(I - \breve{D}_{k+1}M_{k+1}\right)e_{k+1} \tag{38}$$

Obviously, from Eq. (37) and Eq. (38), any value of $K_{k+1}$ satisfies the unbiased condition $E[\hat{e}_{k+1}^Z] = 0$ once $\hat{Z}_{k|k+N-1}$ is unbiased.

*2) Minimum-variance condition*

The error covariance of the estimated state ($\hat{P}_{k+1}^Z$) can be estimated from Eq. (38) as

$$\begin{aligned}\hat{P}_{k+1}^Z &= E[(\hat{e}_{k+1}^Z)(\hat{e}_{k+1}^Z)^T]\\ &= K_{k+1}\Psi_{k+1}K_{k+1}^T + S(K_{k+1}\Upsilon_{k+1}) + \tilde{P}^Z{}_{k+1}\end{aligned} \tag{39}$$

where

$$\Psi_{k+1} \triangleq E\left[\left(\left(I - \breve{D}_{k+1}M_{k+1}\right)e_{k+1}\right)\left(\left(I - \breve{D}_{k+1}M_{k+1}\right)e_{k+1}\right)^T\right] \tag{40}$$

$$= \left(I - \breve{D}_{k+1}M_{k+1}\right)\tilde{R}_{k+1}\left(I - \breve{D}_{k+1}M_{k+1}\right)^T \quad (40)$$

$$\begin{aligned}\Upsilon_{k+1} &\triangleq E\left[-\left(\left(I - \breve{D}_{k+1}M_{k+1}\right)e_{k+1}\right)(\tilde{e}^Z_{k+1})^T\right] \\ &= -\left(I - \breve{D}_{k+1}M_{k+1}\right)\left(\tilde{P}^{Ze}_k\right)^T\end{aligned} \quad (41)$$

The term $\tilde{P}^{Ze}_k \triangleq E[(\tilde{e}^Z_{k+1})(e_{k+1})^T]$ in Eq. (41) is given as

$$\begin{aligned}\tilde{P}^{Ze}_k = &\left(A^*_k\hat{P}^Z_k + J_{k+1}\hat{P}^{ZW^T}_k - G_{k+1}\hat{P}^{ZV^T}_k\right)\Gamma^T_{k+1} \\ &+A^*_k\hat{P}^{ZW}_k\breve{L}^T_{k+1} + A^*_k\hat{P}^{ZV}_k \\ &+J_{k+1}\bar{Q}_k\breve{L}^T_{k+1} - G_{k+1}\bar{R}_{k+1}\end{aligned} \quad (42)$$

The error covariance of the predicted state $\tilde{P}^Z{}_{k+1} = E[(\tilde{e}^Z_{k+1})(\tilde{e}^Z_{k+1})^T]$ can be estimated by using Eq. (37)

$$\begin{aligned}\tilde{P}^Z{}_{k+1} = &A^*_k\hat{P}^Z_k A^{*T}_k + J_{k+1}\bar{Q}_k J^T_{k+1} + G_{k+1}\bar{R}_{k+1}G^T_{k+1} \\ &+S\left(A^*_k\hat{P}^{ZW}_k J^T_{k+1}\right) - S\left(A^*_k\hat{P}^{ZV}_k G^T_{k+1}\right)\end{aligned} \quad (43)$$

By minimizing the trace of $\hat{P}^Z_{k+1}$, the minimum-variance condition that $\boldsymbol{K}_{k+1}$ needs to be satisfied is obtained. Nevertheless, it has been proved that there is more than one solution of $\boldsymbol{K}_{k+1}$ due to the singular matrix $\Psi_{k+1}$ (Gillijns and De Moor 2007).

If singular value decomposition (SVD) is performed on $\Psi_{k+1}$, and let the row vector of $\boldsymbol{S}_{k+1}$ is the singular vector corresponding to the non-zero singular value of $\Psi_{k+1}$, one can get a invertible $S_{k+1}\Psi_{k+1}S^T_{k+1}$. Finally, $\boldsymbol{K}_{k+1}$ can be derived as

$$K_{k+1} = -\Upsilon^T_{k+1}S^T_{k+1}(S_{k+1}\Psi_{k+1}S^T_{k+1})^{-1}S_{k+1} \quad (44)$$

### 2.3 Estimation of the error covariance matrix

Different from the traditional EKF methods, the extra error covariance matrix $\hat{P}^{ZW}_{k+1}$ and $\hat{P}^{ZV}_{k+1}$ are still unknown in the above equations. A recursive form for them is established (Hassanabadi *et al*. 2022).

By substituting Eq. (23) and Eq. (37) into the Eq. (38), one can get

$$\hat{e}^Z_{k+1} = \hat{A}_{k+1}\hat{e}^Z_k + \hat{J}_{k+1}W_{k+1} + \hat{G}_{k+1}V_{k+1} \quad (45)$$

where

$$\begin{aligned}&\hat{A}_{k+1} \triangleq A^*_k - \Phi_{k+1}\Gamma_{k+1};\ \hat{J}_{k+1} \triangleq J_{k+1} - \Phi_{k+1}\breve{L}_{k+1} \\ &\hat{G}_{k+1} \triangleq -G_{k+1} - \Phi_{k+1};\ \Phi_{k+1} \triangleq K_{k+1}\left(I - \breve{D}_{k+1}M_{k+1}\right)\end{aligned} \quad (46)$$

It can be found that $W_{k+2}$ and $V_{k+2}$ have the recursive form as

$$W_{k+2} = \breve{I}_W W_{k+1} + \bar{I}_W W_{k+2};\ V_{k+2} = \breve{I}_V V_{k+1} + \bar{I}_V V_{k+2} \quad (47)$$

where

$$\breve{I}_W \triangleq \begin{bmatrix}0 & I\\ 0 & 0\end{bmatrix};\quad \bar{I}_W \triangleq \begin{bmatrix}0 & 0\\ 0 & I\end{bmatrix} \quad (48)$$

and the similar form can be formulated for $\breve{J}_V, \bar{J}_V$.

Based on Eq. (45) and Eq. (47)

$$\begin{aligned}\hat{P}^{ZW}_{k+1} &= E[(\hat{e}^Z_{k+1})(W_{k+2})^T] \\ &= E\left[\left(\hat{A}_{k+1}\hat{e}^Z_k + \hat{J}_{k+1}W_{k+1} \right.\right. \\ &\qquad \left.\left. + \hat{G}_{k+1}V_{k+1}\right)\left(\breve{I}_W W_{k+1} + \bar{I}_W W_{k+2}\right)^T\right] \\ &= \hat{A}_{k+1}\hat{P}^{ZW}_k\breve{I}^T_W + \hat{J}_{k+1}\bar{Q}_{k+1}\bar{I}^T_W\end{aligned} \quad (49)$$

$$\begin{aligned}\hat{P}^{ZV}_{k+1} &= E[(\hat{e}^Z_{k+1})(V_{k+2})^T] \\ &= E\left[\left(\hat{A}_{k+1}\hat{e}^Z_k + \hat{J}_{k+1}W_{k+1} \right.\right. \\ &\qquad \left.\left. + \hat{G}_{k+1}V_{k+1}\right)\left(\breve{I}_V V_{k+1} + \bar{I}_V V_{k+2}\right)^T\right] \\ &= \hat{A}_{k+1}\hat{P}^{ZV}_k\breve{I}^T_V + \hat{G}_{k+1}\bar{R}_{k+1}\bar{I}^T_V\end{aligned} \quad (50)$$

## 3. Numerical identification by the proposed method

To validate the effectiveness of the proposed method, two numerical validation examples are presented for the identification of structural systems and excitation forces. The first example is the identification of a three-span continuous bridge, with the division of the three substructures, acted an impact load. The second example is more difficult for the identification of a multi-story shear frame structure subjected unknown wind loads via substructure approach. The first example is simulated for the rapid condition assessment of continuous bridges under unknown excitation forces, and the second example is useful for the SHM of buildings subject to unknown wind loading. However, this paper concentrates on proposing a new method for the identification of structural systems and excitation forces using vision-based displacement measurements and substructure approach. Thus, the details of the simulated vision-based displacement measurement, such as the simulation platform and model are not discussed herein.

### 3.1 Identification of a three-span continuous bridge

As illustrated by Fig. 2, a three-span continuous beam bridge is monitored by computer vision. The bridge is discretized with FE model with vertical DOFs in the upper row and rotation DOFs in the lower row. Structural parameters are selected as: each single-span girder bridge is 5 m long with the beam section width $b = 0.25\,m$and height $h = 0.45\,m$, Young's modulus $E = 200\,GPa$ , and the material density $\rho = 7.85 \times 10^6\ \mathrm{kg/m^3}$ . Rayleigh damping with damping coefficient $\alpha = 0.1839$, $\beta = 0.0021$. The structure is divided into three substructures with each span bridge being a substructure. As a demonstrated example, each substructure is divided into 5 beam elements. A vertical impact load $f = 1000\,kN$ is applied to the middle span (13th DOF) of the structure. Structural damage condition is simulated as 10% reduction of the 2nd element stiffness in the 1st (left) span substructure.

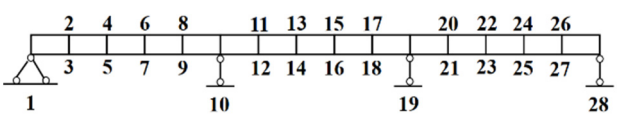


Fig. 2 Three-span continuous bridge

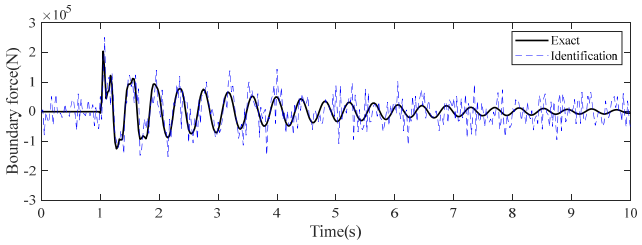


(a) N = 1 (MVU filter)

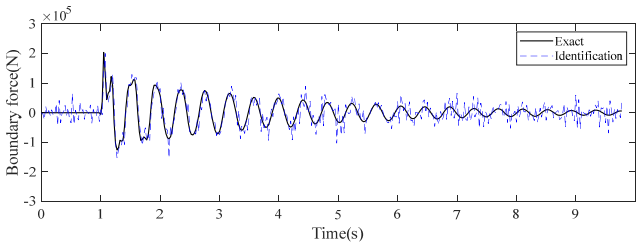


(b) N = 10 in smoothing

Fig. 3 Identified unknown interface force

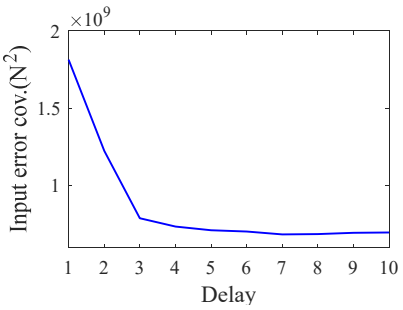


Fig. 4 Effect of delayed steps on the error of the identified input

### *3.1.1 Identification of the unknown interface force in the left span substructures*

For the identification of the left span substructure as the target substructure, structural vertical displacement of each node is monitored by computer vision. To test the robustness of the proposed method against measurement noises, Gaussian white noise data with a 10% standard deviation of each measured signal are added to the observed displacements.

In this case, the unknown substructural interface force is the bending moment at the right end of the substructure. In the identification by the proposed smoothing EKF-UI-WDF algorithm, if only one delayed step (N = 1) is adopted in the smoothing technique, there are still many "burrs" in the identification diagram, but the overall trend is consistent with the real value. When the delayed steps increase to ten steps (N = 10), the identified result is in better agreement with the real value, and the "burrs" are under controlled.

It is worth noting that the dynamic rotational displacement information of interface node is difficult to be accurately observed. The identification of interfacial forces is a necessary step in the substructure identification.

Fig. 4 shows the error reduction of the identified interface force with N. There is a great improvement when N increases at the beginning, but this effect is not so obvious when N is larger than 7. Since the effect of delayed time steps is to smoothing the identification results so that the identification is robust to measurement noises, the selection of the number of delayed steps depends on the smoothing effect on the identification results.

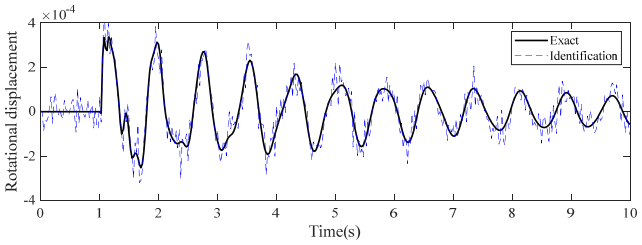


(a) N = 1 (MVU filter)

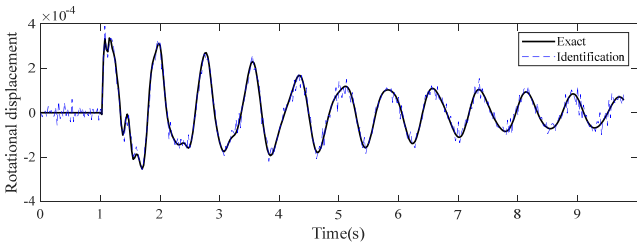


(b) N = 10 in smoothing

Fig. 5 Identified rotational displacement (the 10th DOF)

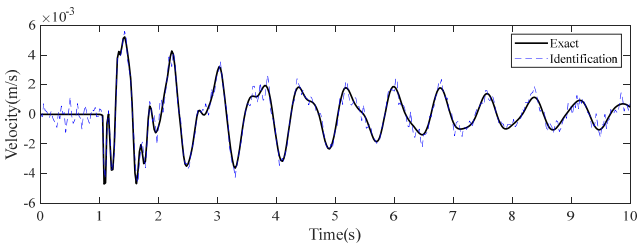


(a) N = 1 (MVU filter)

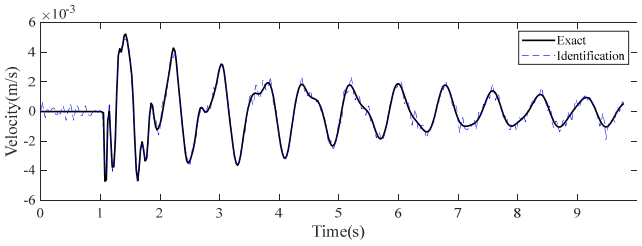


(b) N = 10 in smoothing

Fig. 6 Identified velocity response of the 6th DOF (vertical)

### *3.1.2 Identification of the left span substructural state*

The camera vision only monitors the vertical displacements of all nodes in the left span substructure, so the identified state of rotational displacement and velocity are shown below.

It is known that the measurement of structural dynamic rotational displacement is of difficulty in practice, but the dynamic rotational displacements can be identified by the

proposed method using only vision-based node vertical displacements. Fig. 5 shows the identification of rotational displacement of the 10th DOF in the left substructure. It is seen that when N increases from 1 to 10, the identification of rotational displacement is greatly improved. Errors in several points are unavoidable since a high level of noise has been added to the observed information.

The identifications of velocity responses are better than those of rotational displacements. Fig. 6 shows the identified velocity response of the 6th DOF (vertical), and identification error seems not significant when N = 1 and identification result is also in good agreement when N = 10.

### 3.1.3 Identification of left span substructural parameters

The proposed method can identify not only structural unknown input-state but also structural parameters. Therefore, structural damage can be identified based on the variations of identified structural parameters. Herein, structural damage scenario is simulated as 10% reduction of the 2nd element stiffness in the left span substructure. Fig. 7 shows the identified results for stiffness parameters of an undamaged and the damaged element. It is noted that there are deviations when N = 1 but the identified results converge to the true value quickly when N is set larger than 5 in the smoothing approach.

All the identified element stiffness parameters are summarized and compared with their exact values in Table 1. It can be seen that the identification errors are small.

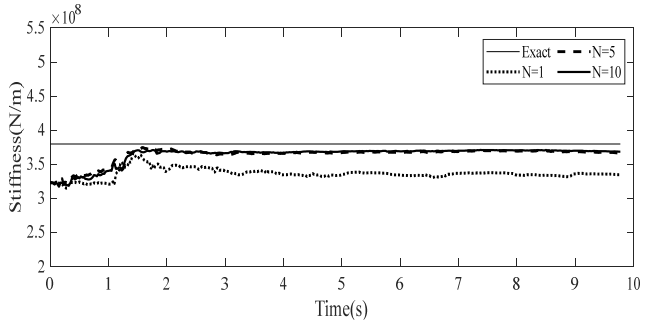


(a) Undamaged element (5th element)

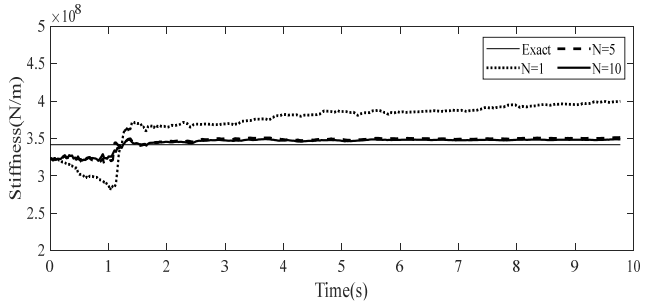


(b) Damaged element (2nd element)

Fig. 7 Identified element stiffness parameters

Table 1 The errors of identified stiffness (N = 10)

| Element | True value ($\times 10^8$N/m) | Identified value ($\times 10^8$N/m) | Error (%) |
|---|---|---|---|
| 1 | 3.80 | 3.66 | 3.53 |
| 2 | 3.42 | 3.47 | -1.81 |
| 3 | 3.80 | 3.72 | 1.88 |
| 4 | 3.80 | 3.70 | 2.59 |
| 5 | 3.80 | 3.80 | 0.01 |

### 3.1.4 Identification of the unknown interface forces in the mid-span substructure

The identification of the mid-span substructure is conducted using the vision-based vertical dynamic displacement responses of all nodes in the mid-span. In this case, there are two unknown substructural interface forces to the mid-span substructure, which are two unknown bending moments at the two supports. Other conditions are the same as those of the left span substructure.

The identification of the two unknown interface forces

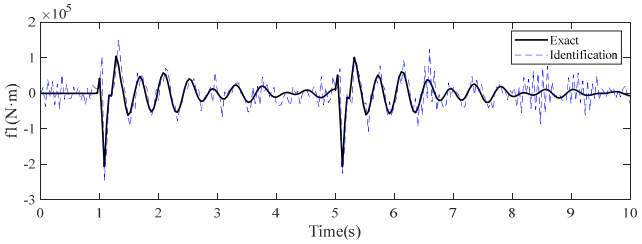


(a) Left interface force (N = 1, MVU filter)

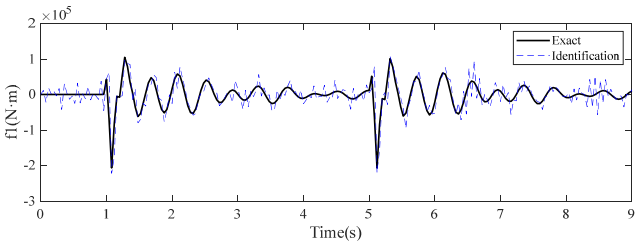


(b) Left interface force (N = 10 in smoothing)

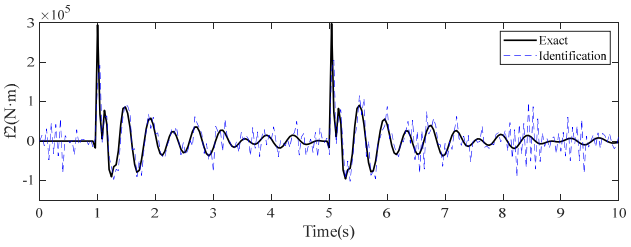


(c) Right interface force (N = 1, MVU filter)

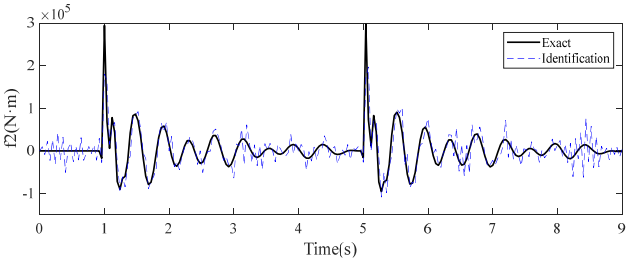


(d) Right interface force (N = 10 in smoothing)

Fig. 8 Identified two unknown interface forces

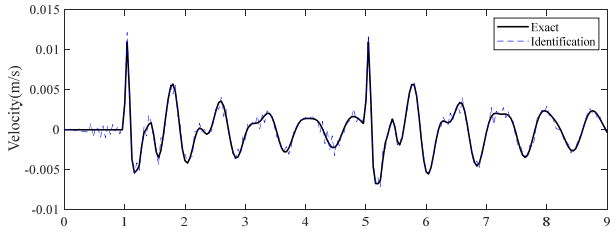


(a) N = 1 (MVU filter)

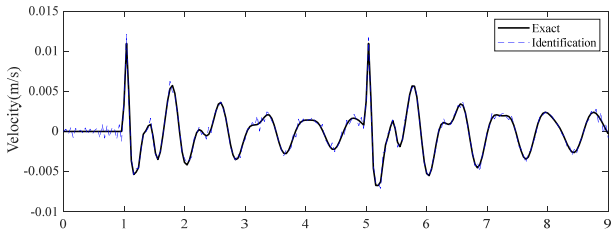


(b) N = 10 in smoothing

Fig. 9 Identified velocity response of the 13th DOF (vertical)

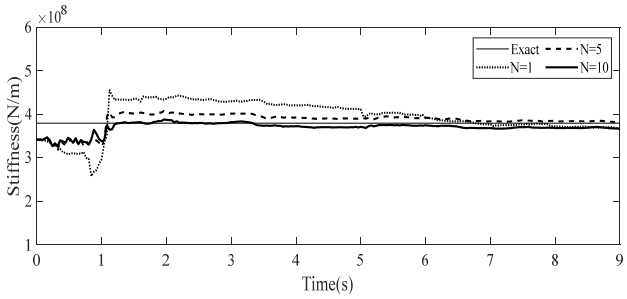


Fig. 10 Identified the 8th element stiffness with different N

of the mid-span substructure is shown in Fig. 8. Analogously, the identified results are improved when N = 10 in smoothing compared with those without smoothing.

#### *3.1.5 Identification of the mid-span substructural state*

Fig. 9 shows the comparisons of the identified velocity responses with the exact value for the cases of N = 1 and N = 10.

#### *3.1.6 Identification of the mid-span substructural parameters*

The line stiffness identification of the mid-span substructure is as follows, and the identification lines under different delayed steps are also given in the Fig. 10.

It can be seen from Fig. 10 that the line stiffness identification value can converge to the true value well under the condition of only observing the dynamic displacement of the vertical freedom of the mid-span.

The identification process of the right span substructure is similar to the left span substructure, which will not be repeated in this section. In addition, from the identification process of the above two substructures, there is no transformation of identified information between each substructure, thus independent parallel identification can be achieved.

Table 2 The error of the identified stiffness (N = 10)

| Element | True value ($\times 10^8$N/m) | Identified value ($\times 10^8$N/m) | Error (%) |
|---|---|---|---|
| 6 | 3.80 | 4.03 | -6.14 |
| 7 | 3.80 | 3.73 | 1.86 |
| 8 | 3.80 | 3.76 | 0.84 |
| 9 | 3.80 | 3.69 | 2.80 |
| 10 | 3.80 | 3.71 | 2.20 |

### *3.2 Identification of a shear frame structure and unknown wind loads*

The identification of a 12-story shear frame and unknown wind loads is used in this section to verify the proposed method. The basic information of the structure is: the height of each story = 2.8 m, the mass of each story $m_i = 1000$ kg, inter-story stiffness $k_i = 6 \times 10^4\ kN/\text{m}$ ($i$ = 1, 2, ..., 12), Rayleigh damping with coefficients $\alpha = 0.0437$, $\beta = 0.0155$. Structural displacements between floors of the building are by computer vision with sampling frequency of 4 Hz. Also, Gaussian white noise with a standard deviation of 1% of each observed displacement response is added to each measured displacement.

Based on the substructural identification approach, the 12-story shear frame is divided into a lower substructure (1st-6th story) and an upper substructure (7th-12th story).

#### *3.2.1 Simulation of the wind loads*

Generally speaking, the vertical dimension of a high-rise buildings is much larger than the horizontal dimension, so only the wind loads along the vertical direction is considered herein. Then, wind load $f(z,t)$ at height $z$ from the ground can be expressed as

$$f(z,t) = \frac{1}{2}\rho_a \mu_s(z) A(z) v^2(z,t) \tag{51}$$

where $\rho_a$ is the density of air, and its value of $1.06\ \text{kg/m}^3$ is adopted. $\mu_s(z)$ is the aerodynamic coefficient at height $z$. $A(z)$ is the frontal area of the building at height $z$, and the value $20\ m^2$ is adopted, $v(z,t)$ is the wind speed which contains the average wind velocity $\bar{v}(z)$ and fluctuating wind velocity $\tilde{v}(z,t)$.

Then

$$\begin{aligned} f(z,t) &= \frac{1}{2}\rho_a \mu_s(z) A(z)[\bar{v}(z) + \tilde{v}(z,t)]^2 \\ &= \frac{1}{2}\rho_a \mu_s(z) A(z)\bar{v}^2(z)\left[1 + \frac{\tilde{v}(z,t)}{\bar{v}(z)}\right]^2 \\ &\approx \bar{f}(z) + \frac{2\bar{f}(z)}{\bar{v}(z)}\tilde{v}(z,t) = \bar{f}(z) + \tilde{f}(z,t) \end{aligned} \tag{52}$$

where, $\bar{f}(z)$ represents the average wind load,$\tilde{f}(z,t)$ is the fluctuating wind load.

Based on the Pearson correlation coefficient, the correlation of fluctuating wind speeds at two neighboring story levels are

Table 3 The correlation of fluctuating wind speeds

| Story | Story 1 and 2 | Story 3 and 4 | Story 5 and 6 | Story 7 and 8 | Story 9 and 10 | Story 11 and 12 |
|---|---|---|---|---|---|---|
| rho | 0.89 | 0.91 | 0.91 | 0.91 | 0.92 | 0.92 |

$$rho(\tilde{v}_n, \tilde{v}_{n+1}) = \frac{\sum_{i=1}^{Nt}(\tilde{v}_{n,i} - \bar{\tilde{v}}_n)(\tilde{v}_{n+1,i} - \bar{\tilde{v}}_{n+1})}{\sqrt{\sum_{i=1}^{Nt}(\tilde{v}_{n,i} - \bar{\tilde{v}}_n)^2 \sum_{j=1}^{N}(\tilde{v}_{n+1,j} - \bar{\tilde{v}}_{n+1})^2}} \quad (53)$$

where $\tilde{v}_{n,i}$ represents the fluctuating wind speed $\tilde{v}$ at the height of the $n$-th story and the time of the $i$-th time point. $Nt$ denotes the number of the time points. $\bar{\tilde{v}}_n$ is the average of the fluctuating wind speed $\tilde{v}_n$. And the correlation results are shown in Table 3.

It can be seen from Table 3 that the correlation between two neighboring fluctuating wind speeds is very strong. Therefore, it is reasonable to assume that the fluctuating wind speeds between two neighboring stories are completely correlated. Then, the number of unknown inputs is greatly reduced in the identification.

It can be seen from Table 3 that the correlation between two neighboring fluctuating wind speeds is very strong. Therefore, it is reasonable to assume that the fluctuating wind speeds between two neighboring stories are completely correlated. Then, the number of unknown inputs is greatly reduced in the identification.

### 3.2.2 Identification of wind loads and interface force in the lower substructure

For the lower substructure, there are three fluctuating wind speeds and one top interface force (equivalent to the inter-story restoring force of the sixth and seventh floors) to be identified.

Fluctuating wind speed $\tilde{v}(z,t)$ is directly identified in the inverse problem, and the corresponding wind load can be reconstructed by substituting the identified value into the Eq. (52). The wind load reconstruction of each floor of the lower substructure is given below. At the same time, the comparison of wind load identification at 1st, 3rd and 6th floor level for 1 step delayed and 10 steps delayed are also given to illustrate the noise reduction effect of the proposed method for wind load reconstruction under the inversion condition based on observed displacement response.

In the case of one step delayed, the wind load composition of each floor has different degrees of "drift", and there are many "burrs" in the whole-time history, indicating that it is difficult to achieve wind load reconstruction only one step behind. In the case of 10 steps delayed, the "drift" phenomenon is eliminated and the

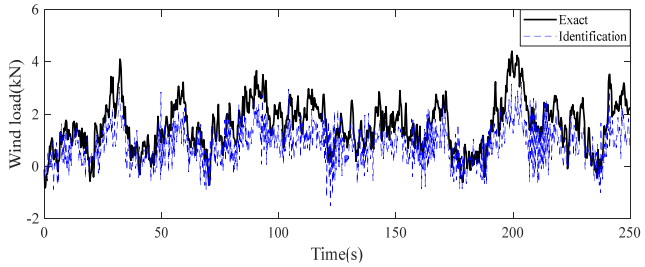


(a) N = 1 (MVU filter)

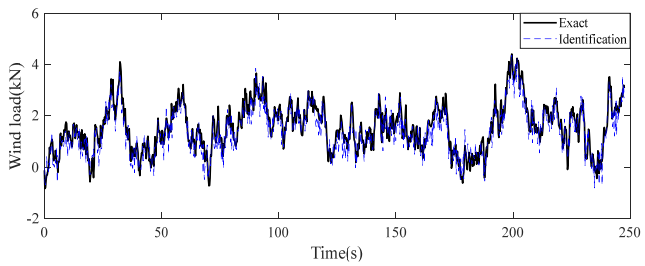


(b) N = 10 (Smoothing)

Fig. 11 Identified wind load at the 1st floor level

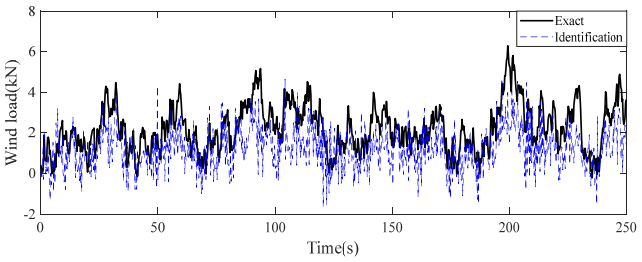


(a) N = 1 (MVU filter)

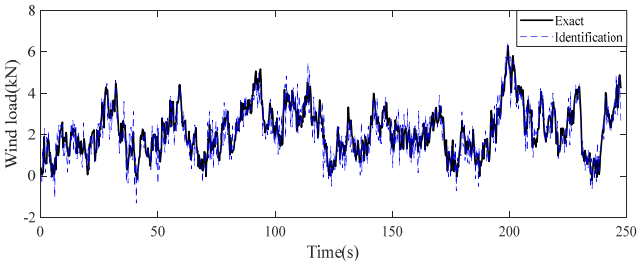


(b) N = 10 in smoothing

Fig. 12 Identified wind load at the 3rd floor level

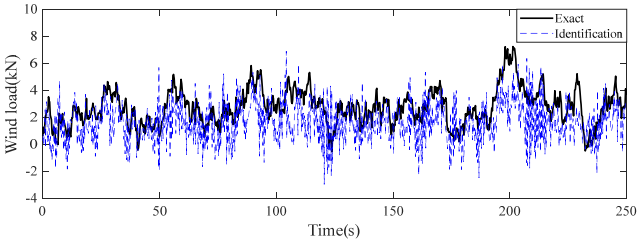


(a) N = 1 (MVU filter)

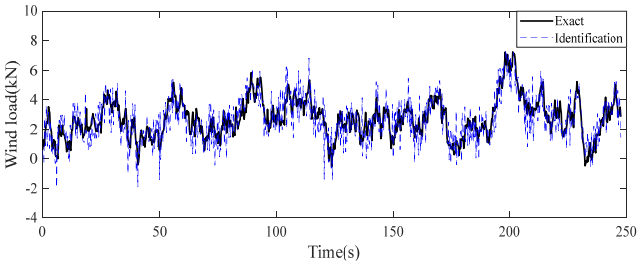


(b) N = 10 in smoothing

Fig. 13 Identified wind load at the 6th floor level

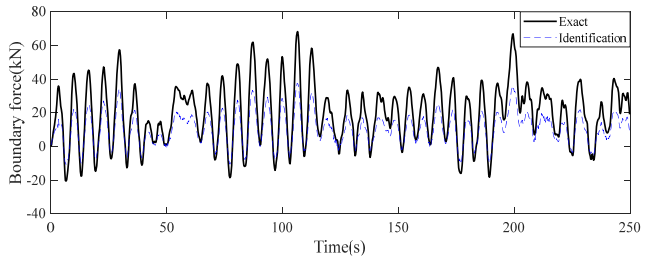


(a) N = 1 (MVU filter)

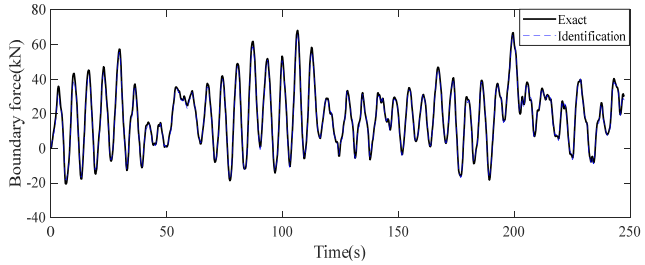


(b) N = 10 in smoothing

Fig. 14 The identified interface force

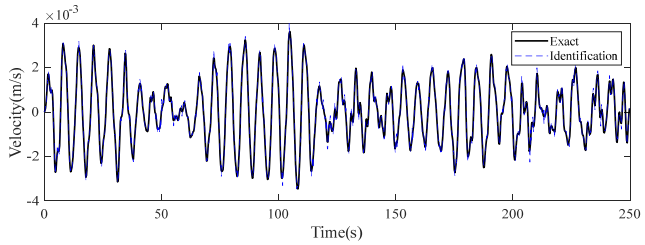


(a) N = 1 (MVU filter)

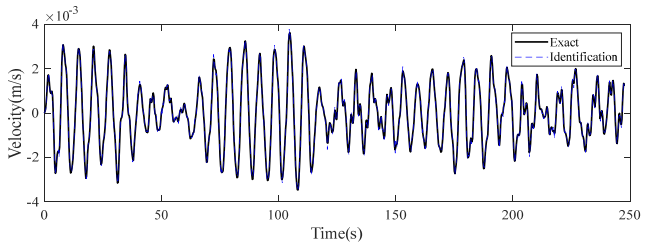


(b) N = 10 in smoothing

Fig. 15 Identified velocity response

"burr" situation is greatly improved. From the perspective of average error, the wind load reconstruction error of each floor is reduced by more than 50% compared with that of one step behind.

The interface forces of the substructure are identified as unknown inputs, but this is not necessary for the evaluation of the substructure, and the identification results are given here as a reference. It can be seen from the Fig. 14(a) that there is no "burr" phenomenon in the recognition of interface force, but there is still a certain "drift" when it is one step delayed.

### *3.2.3 Identification of lower substructural state*

Since all the displacement information of the structure has been obtained, the speed identification situation (taking the fourth floor as an example) is selected here to illustrate

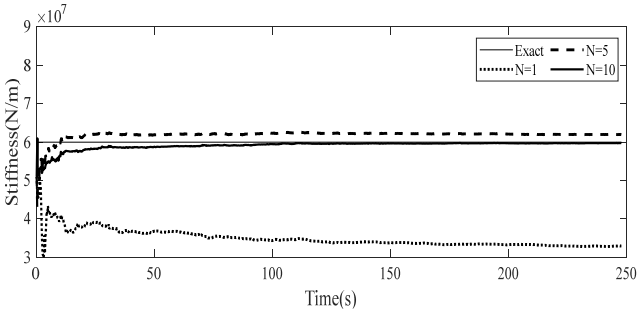


Fig. 16 Identified stiffness using different delayed steps

the state identification situation. The identification of velocity is good, only some points have the slight error when N = 1, and these errors are weakened in the case of N = 10.

### *3.2.4 Identification of the lower substructure parameters*

Similar to the Yuen and Huang (2018a), the structural stiffness matrix can be parameterized as $\boldsymbol{K} = \sum_{i=1}^{N_k} k^{(i)} \boldsymbol{K}_i$, where $k^{(1)}, k^{(2)}$ denote the lower and upper substructural stiffness parameters, respectively, $\boldsymbol{K}_i$ is prescribed nominal stiffness submatrix. In the lower substructure, the initial stiffness value of $k^{(1)}$ is 0.85 times the true value. It is obvious from the Fig. 16 that in the case of N = 1, the recognition line converges to a wrong value and deviates greatly from the real value. When N = 5 and N = 10, the recognition line can converge to the real value quickly. This can also be a good explanation for the phenomenon of large deviation of interface force recognition when N = 1.

### *3.2.5 Identification of wind loads in the upper substructure*

For the upper substructure, there are three unknown wind loads and a low-level interface that need to be identified. The acceleration response of the 6$^{th}$ floor can generally be obtained. That is, the acceleration information of the 6$^{th}$ floor is the known boundary input to the upper substructure as the auxiliary condition.

Some of the identification of wind loads in the upper substructure are given in Figs. 17-19. When N = 10, the identified wind loads in the upper substructure are better than those in the lower substructure. From the perspective of observation information and input information, the upper substructure has 6 observations and 3 unknown inputs. There are 6 observations and 4 unknown inputs in the lower substructure. The unknowns of structural parameters are the same, so the overall identification results of the upper structure are better.

Similar to the lower substructure, when the observation information of the upper substructure is more than 2-3 steps integrated, the error of identified wind load decreases rapidly and tend to be stable. Admittedly, larger noise means that more steps need to be fused. However, in this case, 1% noise is added to the observation information herein, so only a small number of steps need to be fused to achieve the goal of noise reduction.

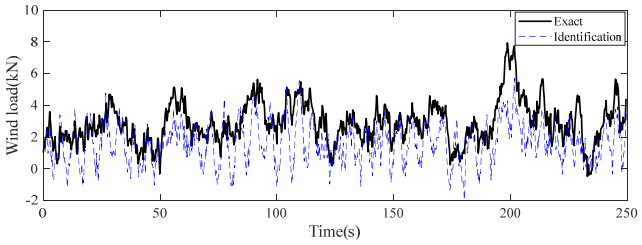


(a) N = 1 (MVU filter)

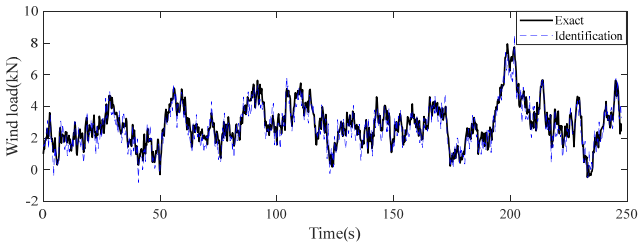


(b) N = 10 in smoothing

Fig. 17 Identified wind load at the 7th floor level

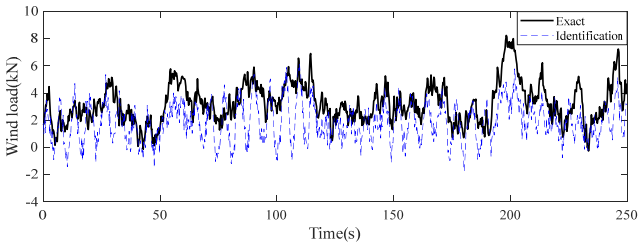


(a) N = 1 (MVU filter)

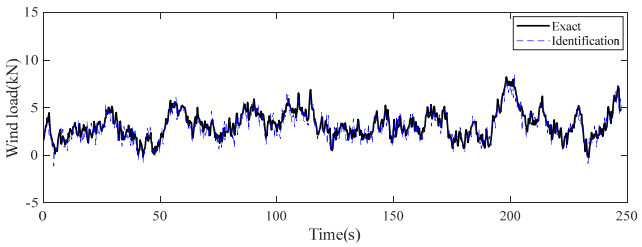


(b) N = 10 in smoothing

Fig. 18 Identified of wind load at the 10th floor level

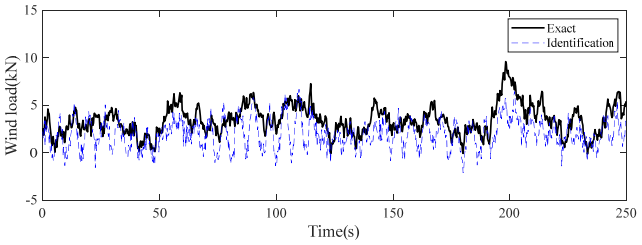


(a) N = 1 (MVU filter)

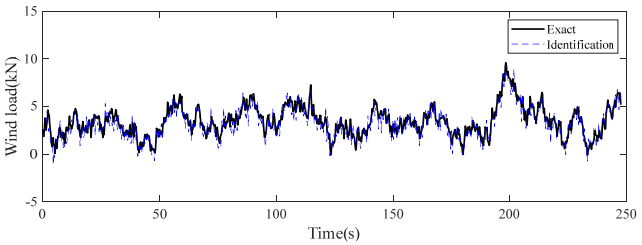


(b) N = 10 in smoothing

Fig. 19 Identified wind load at the 12th floor level

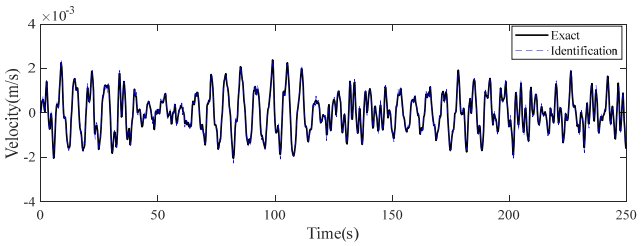


(a) N = 1 (MVU filter)

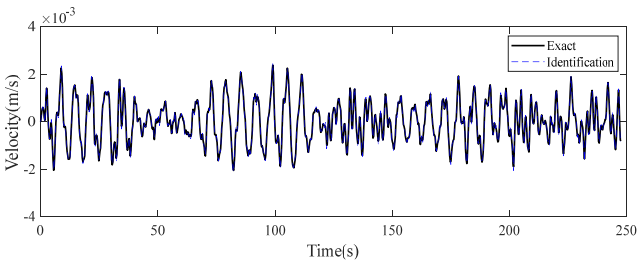


(b) N = 10 in smoothing

Fig. 20 Identified velocity response

### *3.2.6 Identification of the upper substructural state*

Since all the vertical displacement information of the structure has been monitored, the identified velocity (taking the 10th floor as an example) is selected here to illustrate the state identification. It can be seen that the identified state is good since the identified value is highly consistent with the real value. When N = 1, the error covariance is small, and the magnitude is only $10^{-9}$. The influence of noise on state identification is less than that on input identification.

### *3.2.7 Identification of upper substructural parameters*

The parameter to be identified for the upper substructure is the stiffness of each floor, and it is assumed that the stiffness of each floor is equal to the $k^{(2)}$. The initial stiffness value is 0.85 times the real value. When N = 1, the same situation as that of the lower substructure is observed. The recognition line fails to converge to the true value and the deviation is large. When N = 5 and N = 10, the identification lines quickly converge to the real value.

By analyzing the correlation between two levels of fluctuating wind speed, this case assumes a complete correlation between two levels of fluctuating wind speed in the inverse problem, which greatly reduces the number of unknown inputs. Meanwhile, the combination of substructure technology and smoothing EKF-UI-WDF improves the accuracy of identification, and the status identification is almost not affected by noise. The reconstructed wind load is in good agreement with the real

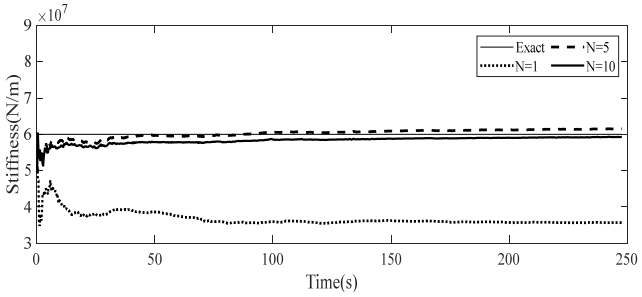


Fig. 21 Identified stiffness with different delay steps

value, and the tracking and identification process of structural parameters is efficient and accurate. Therefore, this case provides a new idea for wind load identification of high-rise buildings, and the proposed method has good robustness.

## 4. Conclusions

In this paper, a novel method based on smoothing extended Kalman filter with unknown inputs without direct feedthrough (smoothing EKF-UI-WDF) is proposed for the simultaneous identification of structural systems and unknown excitation forces using vision-based displacement measurements and substructure approach. The main contribution of the paper are: (1) simultaneous identification of structural systems and unknown excitation forces can be conducted when the unknown excitation forces do not appear directly in the observation equations using vision-based displacement measurements; (2) substructural identification with the smoothing EKF-UI-WDF can solve the identification problem of using limited field of view of monocular vision-based monitoring by parallel identification of each substructure; (3) the smoothing procedure makes the identification results more robust to the measurement noises. Numerical identification examples demonstrate that the identification results of structural state, parameters and unknown excitations are satisfactory by the proposed method.

More validations of the proposed method should be conducted by the identification of other complex structural systems under unknown excitation using vision-based displacement measurements. Also, experimental validations with displacement measurement data obtained from computer visions are necessary. Such works are under taken by the authors.

## Acknowledgments

The research in this paper is supported by the National Natural Science Foundation of China via the grant No. 52178304.

## References

Busca, G., Cigada, A., Mazzoleni, P. and Zappa, E. (2014), "Vibration monitoring of multiple bridge points by means of a unique vision-based measuring system", *Experim. Mech.*, **54**(2), 255-271. https://doi.org/10.1007/s11340-013-9784-8

Chen, J. and Li, J. (2001), "Study on wind load inverse of tall building", *Chinese Quarterly of Mechanics*, (01), 72-77. https://doi.org/10.15959/j.cnki.0254-0053.2001.01.010

Dong, C.Z., Ye, X.W. and Jin, T. (2018), "Identification of structural dynamic characteristics based on machine vision technology", *Measurement*, **126**, 405-416. https://doi.org/10.1016/j.measurement.2017.09.043

Feng, D.M. and Feng, M.Q. (2016), "Vision-based multipoint displacement measurement for structural health monitoring", *Struct. Control Health Monitor.*, **23**(5), 876-890. https://doi.org/10.1002/stc.1819

Feng, D.M. and Feng, M.Q. (2017), "Identification of structural stiffness and excitation forces in time domain using noncontact vision-based displacement measurement", *J. Sound Vib.*, **406**, 15-28. https://doi.org/10.1016/j.jsv.2017.06.008

Feng, D.M. and Feng, M.Q. (2018), "Computer vision for SHM of civil infrastructure: From dynamic response measurement to damage detection - A review", *Eng. Struct.*, **156**, 105-117. https://doi.org/10.1016/j.engstruct.2017.11.018

Feng, W., Li, Q. and Lu, Q. (2020), "Force localization and reconstruction based on a novel sparse Kalman filter", *Mech. Syst. Signal Process.*, **144**, 106890. https://doi.org/10.1016/j.ymssp.2020.106890

Gillijns, S. and De Moor, B. (2007), "Unbiased minimum-variance input and state estimation for linear discrete-time systems", *Automatica*, **43**(1), 111-116. https://doi.org/10.1016/j.automatica.2006.08.002

Hassanabadi, M.E., Heidarpour, A., Azam, S.E. and Arashpour, M. (2022), "A Bayesian smoothing for input-state estimation of structural systems", *Comput.-Aided Civil Infrastr. Eng.*, **37**(3), 317-334. https://doi.org/10.1111/mice.12733

Huang, J.S., Li, X.Z., Zhang, F.B. and Lei, Y. (2021), "Identification of joint structural state and earthquake input based on a generalized Kalman filter with unknown input", *Mech. Syst. Signal Process.*, **151**(9), 107362. https://doi.org/10.1016/j.ymssp.2020.107362

Koh, C.G., Hong, B. and Liaw, C.Y. (2003), "Substructural and progressive structural identification methods", *Eng. Struct.*, **25**(12), 1551-1563. https://doi.org/10.1016/S0141-0296(03)00122-6

Kuddus, M.A., Li, J., Hao, H., Li, C. and Bi, K. (2019), "Target-free vision-based technique for vibration measurements of structures subjected to out-of-plane movements", *Eng. Struct.*, **190**, 210-222. https://doi.org/10.1016/j.engstruct.2019.04.019

Lagerblad, U., Wentzel, H. and Kulachenko, A. (2021), "Study of a fixed-lag Kalman smoother for input and state estimation in vibrating structures", *Inverse Problems Sci. Eng.*, **29**(9), 1260-1281. https://doi.org/10.1080/17415977.2020.1845669

Lei, Y., Yang, N. and Xia, D.D. (2017), "Probabilistic structural damage detection approaches based on structural dynamic response moments", *Smart Struct. Syst., Int. J.*, **20**(2), 207-217. https://doi.org/10.12989/sss.2017.20.2.207

Lei, Y., Lu, J.B. and Huang, J.S. (2020), "Synthesize identification and control for smart structures with time-varying parameters under unknown earthquake excitation", *Struct. Control Health Monitor.*, **27**(10), e2512. https://doi.org/10.1002/stc.2512

Lei, Y., Huang, J.S., Qi, C.K., Zhang, X. and Li, X.Z. (2022), "Parallel substructure identification of linear and nonlinear structures using only partial output measurements", *J. Eng. Mech.*, **148**(7), 04022033. https://doi.org/10.1061/(asce)em.1943-7889.0002117

Li, J. and Hao, H. (2016), "Substructural interface force identification with limited vibration measurements", *J. Civil Struct. Health Monitor.*, **6**(3), 395-410. https://doi.org/10.1007/s13349-016-0157-8

Liu, L.J., Su, Y., Zhu, J.J. and Lei, Y. (2016), "Data fusion based EKF-UI for real-time simultaneous identification of structural systems and unknown external inputs", *Measurement*, **88**, 456-467. https://doi.org/10.1016/j.measurement.2016.02.002

Liu, L.J., Mi, J.N., Zhang, Y.X. and Lei, Y. (2021), "Damage detection of bridge structures under unknown seismic excitations using support vector machine based on transmissibility function and wavelet packet energy", *Smart Struct. Syst., Int. J.*, **27**(2), 257-266. https://doi.org/10.12989/sss.2021.27.2.257

Maes, K., Gillijns, S. and Lombaert, G. (2018), "A smoothing algorithm for joint input-state estimation in structural dynamics", *Mech. Syst. Signal Process.*, **98**, 292-309. https://doi.org/10.1016/j.ymssp.2017.04.047

Maes, K., Karlsson, F. and Lombaert, G. (2019), "Tracking of inputs, states and parameters of linear structural dynamic systems", *Mech. Syst. Signal Process.*, **130**, 755-775. https://doi.org/10.1016/j.ymssp.2019.04.048

Pan, S.W., Su, H.Y., Wang, H., Chu, J. and Lu, R.Q. (2009), "Input and state estimation for linear systems: A least squares estimation approach", In: *2009 7th Asian Control Conference*, pp. 378-383.

Pan, S.W., Xiao, D., Xing, S.T., Law, S.S., Du, P.Y. and Li, Y.J. (2016), "A general extended Kalman filter for simultaneous estimation of system and unknown inputs", *Eng. Struct.*, **109**(2), 85-98. https://doi.org/10.1016/j.engstruct.2015.11.014

Rostami, P., Mahsuli, M., Ghahari, S.F. and Taciroglu, E. (2021), "Bayesian joint state-parameter-input estimation of flexible-base buildings from sparse measurements using Timoshenko beam models", *J. Struct. Eng.*, **147**(10), 04021151. https://doi.org/10.1061/(asce)st.1943-541x.0003095

Spencer, B.F., Hoskere, V. and Narazaki, Y. (2019), "Advances in computer vision-based civil infrastructure inspection and monitoring", *Eng.*, **5**(2), 199-222. https://doi.org/10.1016/j.eng.2018.11.030

Tian, Y.D., Zhang, J. and Yu, S.S. (2019), "Rapid impact testing and system identification of footbridges using particle image velocimetry", *Comput.-Aided Civil Infrastr. Eng.*, **34**(2), 130-145. https://doi.org/10.1111/mice.12390

Wan, Z.M., Wang, T., Li, L. and Xu, Z.C. (2018), "A novel coupled state/input/parameter identification method for linear structural systems", *Shock Vib.*, 2018. https://doi.org/10.1155/2018/7691721

Wang, W.Z., Mottershead, J.E., Siebert, T. and Pipino, A. (2012), "Frequency response functions of shape features from full-field vibration measurements using digital image correlation", *Mech. Syst. Signal Process.*, **28**, 333-347. https://doi.org/10.1016/j.ymssp.2011.11.023

Wang, R.H., Li, J., Chencho, An, S.J., Hao, H., Liu, W.Q. and Li, L. (2021), "Densely connected convolutional networks for vibration based structural damage identification", *Eng. Struct.*, **245**, 112871. https://doi.org/10.1016/j.engstruct.2021.112871

Weng, S., Zhu, H.P., Xia, Y., Li, J.J. and Tian, W. (2020), "A review on dynamic substructuring methods for model updating and damage detection of large-scale structures", *Adv. Struct. Eng.*, **23**(3), 584-600. https://doi.org/10.1177/1369433219872429

Yang, N., Lei, Y., Li, J., Hao, H. and Huang, J.S. (2022), "A substructural and wavelet multiresolution approach for identifying time-varying physical parameters by partial measurements", *J. Sound Vib.*, **523**. https://doi.org/10.1016/j.jsv.2021.116737

Ye, X.W., Dong, C.Z. and Liu, T. (2016), "Force monitoring of steel cables using vision-based sensing technology: methodology and experimental verification", *Smart Struct. Syst., Int. J.*, **18**(3), 585-599. https://doi.org/10.12989/sss.2016.18.3.585

Ye, X.W., Li, Z.X. and Jin, T. (2022), "Smartphone-based structural crack detection using pruned fully convolutional networks and edge computing", *Smart Struct. Syst., Int. J.*, **29**(1), 141-151. https://doi.org/10.12989/sss.2022.29.1.141

Ying, Z.G., Wang, Y.W., Ni, Y.Q. and Xu, C. (2021), "Model-free identification of multiple periodic excitations and detection of structural anomaly using noisy response measurements", *Smart Struct. Syst., Int. J.*, **28**(3), 407-423. https://doi.org/10.12989/sss.2021.28.3.407

Yoon, H., Elanwar, H., Choi, H.J., Golparvar-Fard, M. and Spencer, B.F. (2016), "Target-free approach for vision-based structural system identification using consumer-grade cameras", *Struct. Control Health Monitor.*, **23**(12), 1405-1416. https://doi.org/10.1002/stc.1850

Yuen, K.V. and Huang, K. (2018a), "Real-time substructural identification by boundary force modeling", *Struct. Control Health Monitor.*, **25**(5), e2151. https://doi.org/10.1002/stc.2151

Yuen, K.V. and Huang, K. (2018b), "Identifiability-enhanced Bayesian frequency-domain substructure identification", *Comput.-Aided Civil Infrastr. Eng.*, **33**(9), 800-812. https://doi.org/10.1111/mice.12377

Zhang, J. and Moon, F.L. (2012), "A new impact testing method for efficient structural flexibility identification", *Smart Mater. Struct.*, **21**(5). https://doi.org/10.1088/0964-1726/21/5/055016

Zhang, J., Guo, S.L. and Zhang, Q.Q. (2015), "Mobile impact testing for structural flexibility identification with only a single reference", *Comput.-Aided Civil Infrastr. Eng.*, **30**(9), 703-714. https://doi.org/10.1111/mice.12112